Bull. Chem. Soc. Ethiop. **2024**, 38(1), 199-212.
DOI: https://dx.doi.org/10.4314/bcse.v38i1.15

ISSN 1011-3924
Printed in Ethiopia
Online ISSN 1726-801X

SYNTHESIS AND CHARACTERIZATION OF ACTIVATED CARBON FROM *ASPHODELUS MICROCARPUS* IN TWO STEPS

Ourred Mohammed[1*], Kaid Mhamed[2] and Merine Houaria[3]

[1]Department of Chemistry, Faculty of Exact Sciences, Djillali Liabès University, Sidi Bel Abbes, Algeria
[2]Physico-chemical Studies Laboratory (LEPC), Faculty of Science, Moulay Tahar University, Saida, Algeria
[3]Laboratory of Organic Physical and Macromolecular Chemistry, Faculty of Exact Sciences, Djillali Liabes University, Sidi Bel-Abbes, Algeria

(Received October 31, 2022; Revised September 19, 2023; Accepted September 20, 2023)

ABSTRACT. The aim of the present work was to prepare an activated carbon from new precursor *Asphodelus microcarpus* using KOH as an impregnating agent, in two steps and in the absence of nitrogen. Its preparation requires a pre-carbonization at 500 °C for 60 min in order to obtain the char. Then activation of the char is realized by using KOH using as activating agent variable impregnation ratio: char/activating agent. Calcination is then carried out at 750 °C and 850 °C for 1 hour without azote. The determination of the optimum conditions is carried out by measuring the iodine number and that of methylene blue. The characterization of the chosen product is carried out by the following techniques: BET, FTIR-ATR, SEM and DRX. Under optimum conditions with mass ratio 1:4 at 750 °C (the calcination temperature), the specific surface area is equal to 1025.75 $m^2.g^{-1}$ and we obtain micro-meso activated carbon. The adsorption kinetics of dye chosen agrees with the pseudo-second-order model, and it appears that Freundlich (two parameters model) and Redlich-Peterson (three parameters model) describe better the adsorption data. Error analysis also showed that the Freunlich model better described the adsorption of Eriochrome Black T compared with the three parameter models.

KEY WORDS: *Asphodelus microcarpus*, Two-stage activation process, Chemical activation, Adsorption, Dye

INTRODUCTION

Different precursors like wood, lignite, fruit shell, polymers, plants can produce activated carbon [1, 2]. In 1970s, researchers have synthesized for Amoco Corporation USA (The Amoco Corporation is an American chemical and oil company, founded by Standard Oil Company in 1889), an activated carbon with high surface area. They use KOH as activation agent and petroleum coke, coal as precursors [3]. They found that the materials prepared are highly microporous when compared with those prepared with $ZnCl_2$ or H_2SO_4 [4].

The chemical activation method can be achieved in one or two steps. One-step activation consists of impregnating the biomass (the precursor) with the activating agent and subjecting the impregnated biomass to carbonization. The second one requires the initial carbonization of the precursor at temperature ranging from 300 °C to 600 °C. There decomposition leads to release of volatile products and tars giving rise to poorly developed porosity. The next step involves the impregnation of the precursor pre-carbonized with chemical activating agent, followed by a carbonization at a temperature ranging from 700 °C to 900 °C [5]. The activated carbon obtained has a very developed porosity. For examples, Kousar Jahan and his collaborators conducted a study in order to develop an activated carbon from KOH and from pre-carbonized chickpea peel residue for removal of synthetic dye from drinking water [6]. The next example is the study of El Habib Yahia *et al*. [7]. This study focuses on the preparation and characterization of activated

*Corresponding author. E-mail: abacij25@gmail.com

carbon derived from Argan paste cake through carbonization at 300 °C followed by activation at 800 °C utilizing KOH as the activation agent [7].

The study of Qui and his collaborators is another example [8]. They conducted a study on the KOH impregnation of corn straw first carbonized at a temperature of 500 °C then impregnated and finally exposed to 750 °C for one hour. The authors noted that the areas and volume of the mesopore increased significantly with an increase in the rate of impregnation [8].

Therefore, the objective of this work is to study the effect of the activation agent/biochar precursor ratios with that of the temperature on the characteristics of the activated carbon obtained from a new precursor: *Asphodelus microcarpus* and see its performance in adsorbing an anionic azo dye dissolved in water. In other words, to find the optimal conditions so that the percentage of mesopores as well as the pore volume of the activated carbons prepared are sufficiently high to optimize the quantity of adsorbed azo dye used as effluent.

EXPERIMENTAL

Materials

Locally obtained, the plant was thoroughly washed to remove dirt and other unwanted materials and then air dried. Potassium hydroxide (KOH), iodine (I_2), methylene blue, EBT (Eriochrome Black T) were purchased from Sigma-Aldrich. HCl (37%) from Fluka, (NaOH, $NaHCO_3$, Na_2CO_3) from Sigma-Aldrich.

Activated carbons synthesis

The synthesis protocol followed the work of M.J.B. Evans *et al.* [9] in the absence of nitrogen. The plant was first washed with distilled water and air dried. Subsequently, the plant has been pyrolyzed at 500 °C for one hour with heating rate of 10 °C.min^{-1}. The biochar obtained was named B3. For the activation, B3 was mixed with KOH in a KOH/B3 ratio equal to 1:1; 1:2; 1:3 and 1:4.Then each mixture was carbonized at 750 °C and at 850 °C (only 1:3 and 1:4) for one hour with a heating rate equal to 10 °C/min. The adsorbent obtained was washed with 1 M HCl solution, then with distilled water until a neutral pH. In the end, it was dried in an oven at 80 °C for 24 hours. The measurement of the iodine number and methylene blue number were used for pre-evaluation of the developed surface and the porosity obtained by varying the mass ratio between the impregnating agent and the biochar. The effect of the temperature was also studied. The activated carbon obtained was named C3-1/x with x = 1, 2, 3, 4. The iodine number is a parameter widely used for test on an activated carbon. It gives an estimate of its specific surface area and its porosity [10]. The methylene blue is an indicator of the capacity of activated carbon to adsorb medium and large molecules [10]. The Boehm method was also used for the determination of the acid-basic groups [11]. The pH point of zero charge was also determined [12].

Characterization techniques

The texture characteristic of the chosen product was determined by measuring the N_2 adsorption-desorption isotherm at 77 K, using a NOVA 1000 apparatus (Quantachrome instrument, USA). The product was degassed prior at 150 °C under vacuum in order to remove residual moisture. The specific surface area and total pore volume were then determined by the B.E.T method [13]. De Boer method give the ultra-micro pore volume and the external surface area by using the adsorbed volume (V_{ads}) curve as a function of t-plot with t being the thickness of the adsorbed layer and which was obtained from the relation given by Harkin-Jura [14]. Dubinin-Radushkevich (DR) method gives for its part the micro pore volume [15]. The estimation of the pore size

distribution was determined automatically by BJH model [16]. The functional groups present in the surface were determined by using FTIR spectrometer (Brucker Alpha equipped with diamond, USA in wave number range 4000-400 cm^{-1}. The X-Ray diffraction diagram of the product chosen was obtained on a X-ray powder system from the Bruker model, USA. Samples were scanned from 5° to 80° using Cu-$K_{\alpha 1}$ (λ = 1.54060 Å) and $K_{\alpha 2}$ (λ = 1.54439 Å) radiation at 40 kV and 25 mA. The identification of phases and crystal structures is obtained by comparing with databases of files such as PDF-2 2004. The surface morphology of the sample was examined using a model scanning electron microscope (SEM): high voltage 0.2-30 kV; Emitter Schottky Type, Quanta 250 USA. The amount of dye left in the filtrate was determined by a UV-Vis spectrophotometer UV-Vis optizen 3220 South Korea.

Adsorption study

Batch adsorption experiments were carried out by stirring the solution containing the effluent and a certain amount of the adsorbent in a tightly closed flask for a certain time. All parameters were studied (time of contact, speed of agitation, pH). Then the amount of dye left in the filtrate solution was determined by spectrophotometry ultraviolet-visible (UV-Vis) after separation the solid from the liquid by a centrifugation at 5000 rpm for 5 min.

Adsorption isotherm

In order to model our results, five models were used: the Langmuir, Freundlich, Redlich-Peterson, Sips and Langmuir-Freundlich models [17].

Table 1. The models applied and their equations.

Isotherm-kinetic	Equation of isotherm (nonlinear form) and equation of kinetic models (linear form)		References
Isotherm			
Langmuir isotherm	$Q_e = \frac{a*b*Ce}{1+b*Ce}$	(1)	[17]
Freundlich isotherm	$Qe = K_F C^{1/n}$	(2)	[17]
Redlich-Peterson isotherm	$Qe = \frac{a*Ce}{1+b*Ce^c}$	(3)	[17]
Sips isotherm	$Qe = \frac{Qs*Ks*C^\beta}{1+Ks*C^\beta}$	(4)	[17]
Langmuir-Freundlich	$Qe = \frac{Qm*(K*C)^\beta}{1+(K*C)^\beta}$	(5)	[17]
Kinetic model			
Pseudo first-order :	$Ln(q_e - q_t) = Lnq_e - k_1 t$	(6)	[18]
Pseudo second-order	$\frac{t}{q_t} = \frac{1}{k_2 q_{max}^2} + \frac{t}{q_{max}}$	(7)	[19]
Elovich model	$q_t = \frac{1}{b} Log(ab) + \frac{1}{b} Log\, t$	(8)	[19]
Weber and Morris model	$q_t = k_{i,d} * t^{1/2} + C_i$	(9)	[19]

where: (1): C_e (mg. L^{-1}) is the adsorbate concentration at equilibrium; a = Q_{max} ($mg.g^{-1}$) is the maximum amount of adsorbate; Q_e ($mg.g^{-1}$) is the adsorbate amount of adsorbate and b ($L.mg^{-1}$) is the Langmuir adsorption constant. (2): K_F and n are both constant of Freundlich isotherm. (3) a: is Redlich-Peterson isotherm constant ($L.g^{-1}$); b is constant ($L.mg^{-1}$); c is Redlich–Peterson isotherm exponent that lies between 0 and 1; C_e is the equilibrium liquid-phase concentration of the adsorbent ($mg.L^{-1}$) and Q_e is the equilibrium adsorbate loading on the adsorbent ($mg.g^{-1}$). (4): Q_s and K_s ($L.g^{-1}$) are Sips isotherm constant; β is Sips isotherm exponent that lies between 0 and 1. (5): Q_m is Langmuir-Freundlich maximum adsorption capacity (mg/g); K is the equilibrium constant for heterogeneous solid and β is the heterogeneous parameter which lies between 0 and

1. (6): the rate constant for first-order is k_1 (min^{-1}) and q_e (mg/g) denote the amount of dye at equilibrium adsorption. (7): k_2 ($g.mg.min^{-1}$) represent second-order rate constant; q_{max} ($mg.g^{-1}$) denote the maximum amount dye adsorption and q_t ($mg.g^{-1}$) is the amount of dye adsorbed at time t (min.) and $h = k_2.q_{max}^2$ is the initial sorption rate ($mg.g^{-1}.min^{-1}$). (8): *a* and *b* are the constants of this model obtained from the slope and intercept of the linear plot of q_t versus Log *t*. (9): $k_{i,d}$ (mg. $g^{-1}.min^{-0.5}$) is the rate parameter of stage *i*; C_i the intercept of stage *i*. It gives an idea about the thickness of boundary layer [26, 27].

Adsorption kinetic

The pseudo-first-order model [18], the pseudo second-order model [19] and Elovich model were tested to fit the batch experimental data [19]. The intra-particle diffusion model was also applied in order to examine the mechanisms of adsorption for dye removal by the adsorbent [19] (Table 1).

Thermodynamic studies

The next relation is obtained from the relation of Gibbs-Helmhotz and from that of Van't Hoff:

$$LnK_d = Ln\frac{q_e}{c_e} = Ln\frac{(c_0 - c_e)V}{m * c_e} = \frac{\Delta S}{R} - \frac{\Delta H}{R} * \frac{1}{T} \quad (10)$$

where K_d ($L.g^{-1}$) is the distribution coefficient; c_0 ($mg.L^{-1}$) is the initial concentration of adsorbate; c_e ($mg.L^{-1}$) is the equilibrium concentration of adsorbate; V (L) is the volume of solution of adsorbate; m (g) is the mass of the adsorbent; q_e (mg. g^{-1}) is the equilibrium quantity of adsorbate adsorbed per unity of mass of adsorbent. *R* universal gas constant (8.314 $J.mol^{-1}.K^{-1}$). ΔG, ΔH, ΔS, q_e and *T* are free energy, enthalpy, entropy, equilibrium quantity of adsorbate per mass unity of adsorbent and absolute temperature, respectively. The enthalpy ΔH and entropy ΔS are obtained from equation (10). The Arrhenius relation was used to evaluate the activation energy E_a:

$$Lnk_2 = LnA - \frac{E_a}{R} * \frac{1}{T} \quad (11)$$

where: k_2 is the rate constant obtained from the appropriate kinetic model; E_a ($kJ.mol^{-1}$) is the Arrhenius activation energy of adsorption; *A* is the Arrhenius factor; *R* is the universal gas constant (8.314 $J.mol^{-1}.K^{-1}$); and *T* (K) is the absolute temperature. When Lnk_2 is plotted against $1/T$, a straight line with slope of $-E_a/R$ is obtained.

Data analysis

The validity of the isotherm models was checked by plotting equations with the experimental data and applying non-linear regression. The optimization procedure requires an error function able to evaluate the goodness-of-fit of the experimental data to the proposed models [17]. In the present study, the applicability of all model isotherm equations was estimated using eight nonlinear error functions, namely the coefficient of determination R^2, the sum square of errors (ERRSQ/SSE), the average relative error (*ARE*), the root mean square error (*RMSE*) [20], the chi-square test $\chi 2$, the hybrid fractional error function (HYBRID), Marquardt's percent standard deviation (MPSD) and the sum of absolute errors (EABS/SAE) [21]. The procedure of normalizing and combining error results were also used for the determination of the "sum of normalized errors: SNE. The values obtained are then compared in order to evaluate every adsorption isotherm model used [21]. The calculations were made by the software origin 9.

RESULTS AND DISCUSSION

Synthesis

The results for iodine number and methylene blue index are given in Table 2.

Table 2. Effects of ratio KOH/Biochar and temperature of the activation on the yield, iodine and methylene blue number value of each product prepared.

C3 Ratio : KOH/B3 Temperature (°C)	Parameters and results					
	1:1 750	1:2 750	1:3 750	1:4 750	1:3 850	1:4 850
Yield after calcination (%)	30	23.33	18.9	17.5	7.5	7.5
Iodine number ($mg.g^{-1}$)	101.5	329.9	837.5	1002.5	977.1	977. 3
Methylene blue index ($mg.g^{-1}$)	0	0	390.6	399.6	399.7	399.8

The product with the highest iodine number value corresponding to methylene blue index equal to 399.59 mg g^{-1} was chosen (Table 2).

Boehm method

Amounts of surface acidic and basic functional groups such as –COOH; -OCO; -OH are: carboxylic acids (–COOH): 5.0305 $mmol.g^{-1}$; lactones (–COO–): 4.47 $mmol.g^{-1}$; phenols: (–OH) 0.405 $mmol.g^{-1}$ and 20.14 $mmol.g^{-1}$ as basic function. The basic functions are largely superior to the acid functions located at the surface.

Point of zero charge

The point of zero charge is 7.04: approximately neutral.

Characterization of C3-1/4

BET study

According to the IUPAC classification, the isotherm obtained is a type IV and its hysteresis loop is type H4. So we have a micro-mesoporous activated carbon. As it can be seen in Table 3, the surface of mesopores obtained from t-plot is higher than the surface of micropores. Also the proportion of microporous volume obtained from the same method represents only 3.12% from the total volume (only the ultramicropore volume: 0.7 nm) but the D-R method (Dubinin-Radushkevich method) gives 54.53%. The mesoporosity is analyzed by the BJH method. It gives S_{BJH} = 264.418 $m^2.g^{-1}$ and V_{BJH} = 0.313 $cc.g^{-1}$. The valor of S_{BJH} is very low than obtained from t-plot. On the other word, if $S_{BJH} < S_{BET}$ so some proportion of porosity of our activity carbon is microporous. Before concluding, first the BJH method only takes into account the phenomenon of capillary condensation which begins at a certain relative pressure, and then it assimilates the pores to cylinders. This is not the case with the porosity of our adsorbent.

Table 3. Textural characteristics of C3-1/4.

Sample		C3-1/4
S_{BET}		1025
V_{DR}		0.42
t-plot	V_{micro}	0.024
	S_{ext}	91.81
	S_{micro}	107.7
	S_{meso}	824.7
Percentage	DR	54.53%
	t-plot	3.12%
BJH method	V_{BJH}	0.313
	S_{BJH}	264.4
V_{total}		0.7702

S_{BET}, S_{ext}, S_{micro}, S_{meso} and S_{BJH}: $m^2.g^{-1}$ and V_{DR}, V_{micro}, V_{BJH} and V_{total}: $cc.g^{-1}$.

FTIR analysis

The chemical functional groups present in our product (Figure 1(a)) have been determined by FTIR- ATR spectroscopy. The spectrum obtained is interpreted on the basis of the characteristic vibration frequencies of the most common functional groups. The bands at 1559.5 cm^{-1} and 1552.2 cm^{-1} can be attributed to C=C in aromatic rings [22, 23]. The bands at 1752.8 cm^{-1} and at 1708.1 cm^{-1} can be attributed to the vibration of carbonyl group C=O present in many functional groups like carboxylic acid, lactone, quinone. Also two bands at 1064.3 cm^{-1} and at 1048.8 cm^{-1} are present. We can attribute this to the stretching vibrations of the C–O bonds of esters, phenols, alcohols or ethers [23]. In the end, the bands which appear in 2800-2900 cm^{-1} are attributed to the stretching vibrations of the C–H bonds of the methylene groups –CH2– [23] and bands which appear at 553.6 cm^{-1} and in 746.9-880 cm^{-1} indicate a presence of C–H out-of-plane bonding in benzene derivatives [24] (figure 1(a)).

XRD analysis

The X-ray diffractogram of our sample exhibited two peaks characteristic: at 21° and at 43° due to the presence of SiO_2 and graphite, respectively. The structure of our sample is therefore amorphous [25] (Figure 1(b)).

SEM analysis

The photos in Figure 1((c), (d) and (e)) represent the analysis of our activated carbon C3-1/4 obtained. The micrograph of the surface of our material shows that its surface has the appearance of sheets, with highly porous morphology due to chemical activation.

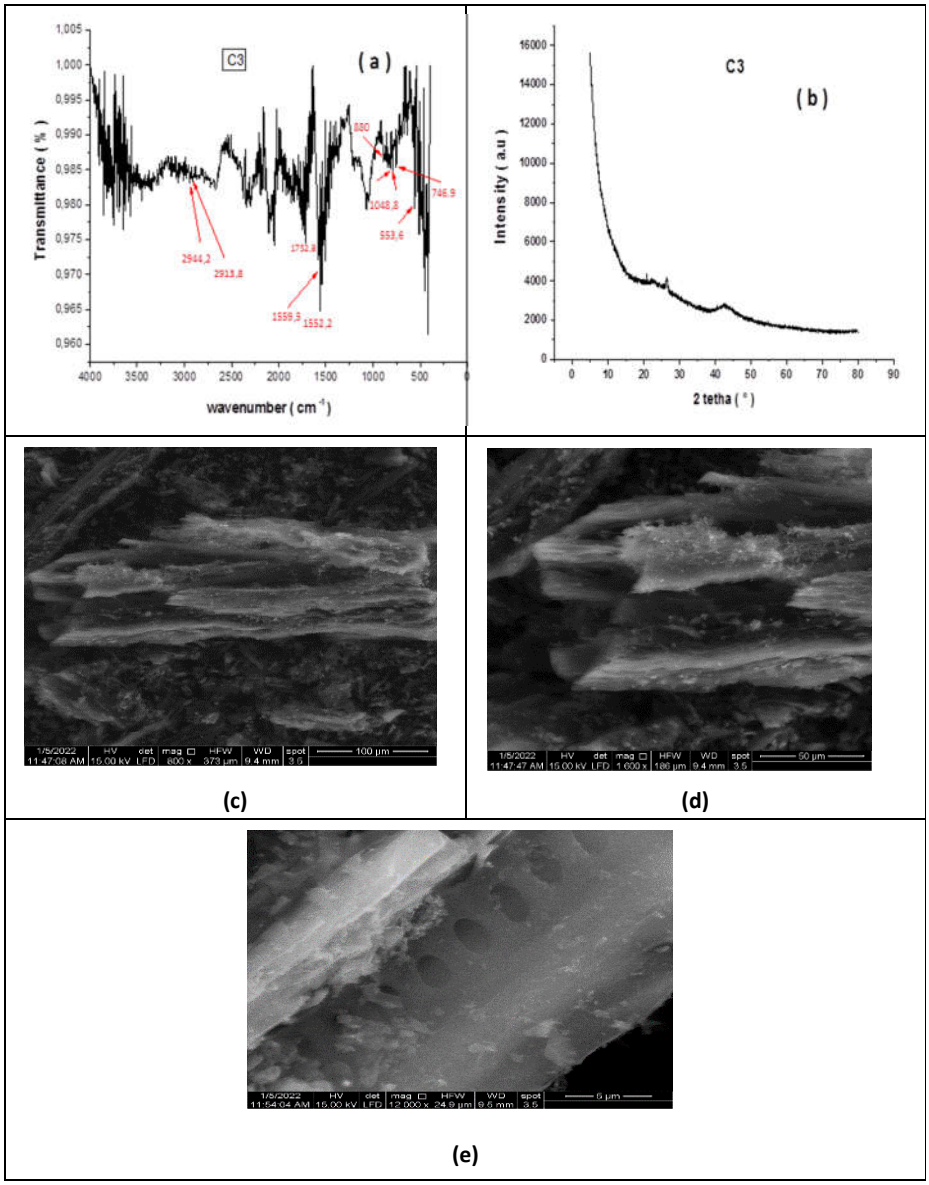

Figure 1. (a) FTIR Spectra of C3; (b) XRD diagram of C3; SEM of C3-1/4: (c)*800; (d)*1600 and (e)*12000.

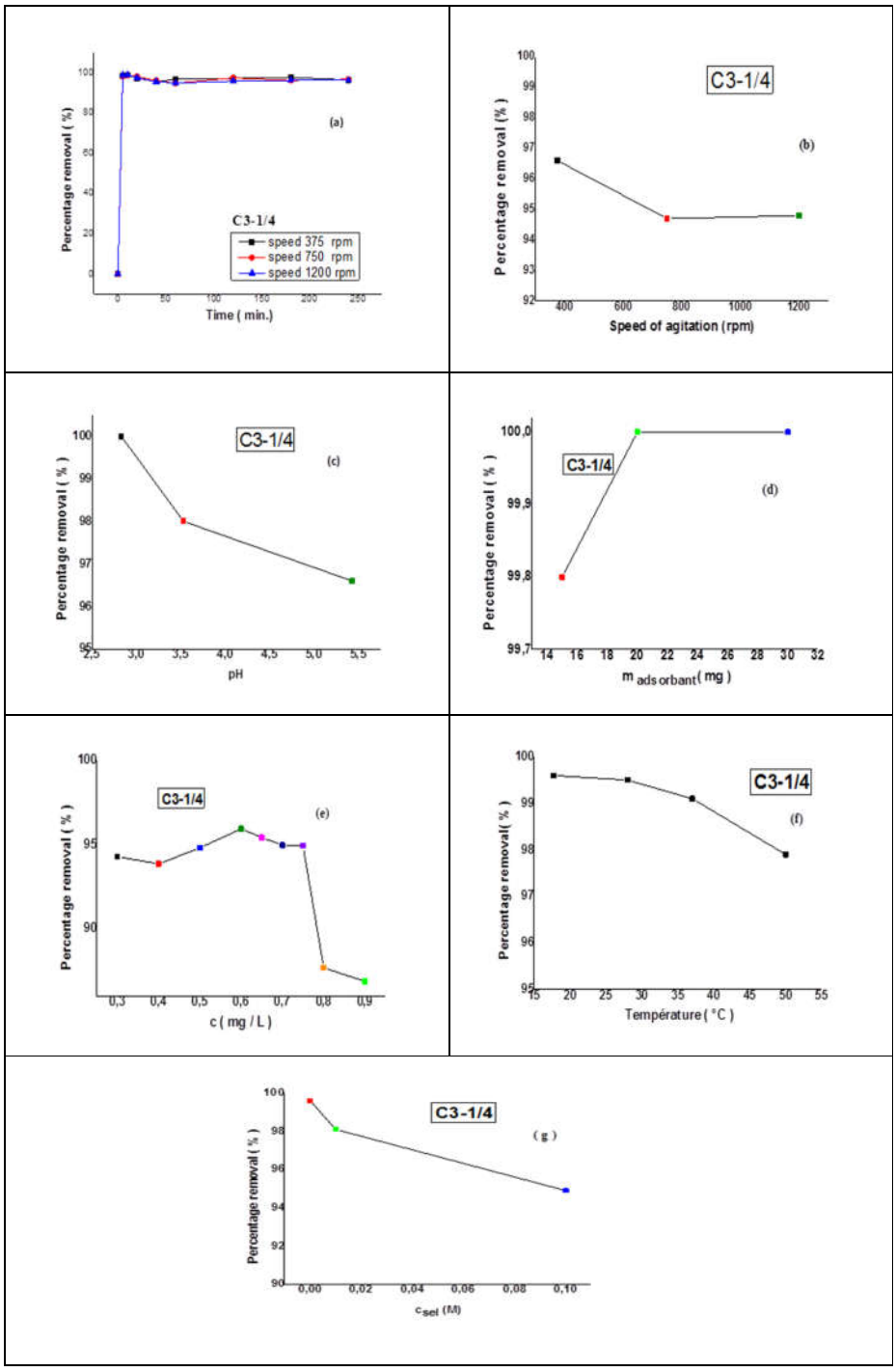
(a)
Percentage removal (%)
C3-1/4
speed 375 rpm
speed 750 rpm
speed 1200 rpm
Time (min.)
C3-1/4
(b)
Percentage removal (%)
Speed of agitation (rpm)
C3-1/4
(c)
Percentage removal (%)
pH
C3-1/4
(d)
Percentage removal (%)
m adsorbant (mg)
C3-1/4
(e)
Percentage removal (%)
c (mg / L)
C3-1/4
(f)
Percentage removal(%)
Température (°C)
C3-1/4
(g)
Percentage removal (%)
c sel (M)

Figure 2. (a) and (b) Effect of the time of contact and the speed of agitation; (c) Effects of initial pH; (d) Effect of quantity of adsorbent; (e) Effect of initial concentration; (f) Effect of temperature; and (g) Effect of ionic strength. The optimal conditions of adsorption 60 min; 375 rpm; pH = 2.83; 15 mg; C_0 = 0.6 g.L^{-1}; 20 °C.

Dye removal studies

The effect of contact time was studied from 5 to 240 min with three speeds of agitation (Figure 2). These two effects are shown in Figure 2 (a) and (b). The equilibrium is obtained after 60 min of agitation and the speed 375 rpm gives the higher yield. The effect of the solution pH (the second effect) was studied by varying the initial pH of the solution of dye (Figure 2 (c)). The others parameters were fixed. If the surface is positively charged (since solution pH < pH_{pzc}), the adsorption capacity of adsorbent increase due to an enhancement of electrostatic attraction between dye molecules charged negatively and surface of adsorbent cited above. As can be seen from Figure 2 (c), the maximum adsorption of EBT onto the adsorbent was obtained at pH = 2.83. Dye removal was also investigated by varying the amount of adsorbent. The removal percentage of dye for 15, 20 and 30 mg are 99.8%, 100% and 100%, respectively. So we obtain approximately the same removal percentage with only 15 mg. This valor has sufficient number of active sites (Figure 2 (d)). Many concentrations were chosen to study the effect of initial concentration of dye (Figure 2 (e)). The first four concentrations give almost the same removal percentage (99.8%, 99.96%, 98.9 % and 99.6%) but the quantities adsorbed per gram of adsorbent are equal to 398.3, 329.7, 266.6 and 199.6 mg.g^{-1} when the initial concentrations is equal to 0.6, 0.5, 0.4 and 0.3 g. L^{-1}, respectively. The decrease of the removal percentage begins after 0.6 g.L^{-1}: this concentration has the maximal valor of the removal percentage (higher percentage removal) of dye. The temperature has also its effect in the quantities of dye adsorbed (Figure 2: (f)). The removal percentage decrease when the temperature increase from 17.7 °C to 50 °C (99.6% at 17.7 °C; 99.5% at 28 °C; 99.1% at 37 °C and 97.9% at 50 °C after 60 min of contact). At the end, the effect of ionic strength on dye sorption was studied with a solution of sodium chloride (0.1 M and 0.01 M). The increase of the concentration of a salt decreases the removal percentage of a dye. These results suggest that the sorption of EBT is partially ionic strength dependent, indicating the role of electrostatic attraction in the sorption system at these conditions (Figure 2 (g)).

Adsorption isotherm models and error analysis

In general, if plus values of errors functions are low that means there is more agreement between the experimental and calculate data. The result of the non-linear regression method (Table 4 (a) and (b)) revealed that the Freundlich model has higher correlation coefficient and have value of n greater than unity (n =1.56) [17, 26]. This isotherm (two parameters isotherm) fit the data in the best way for C3-1/4 (high value of R^2 and low SNE, SSE, RMSE, HYBRID, ARE, EABS, MPSD).

Also from Table 4 (a) and (b), Redlich-Peterson isotherm overlapped and seemed to be the best-fitting model for the experiment for this sample. Therefore, by comparison, the order of the isotherm best fits of experimental data in this study is Redlich-Peterson > Freundlich-Langmuir > Sips for three parameter isotherms and Freundlich > Langmuir for two parameters isotherms. These models (three parameters) are each an empirical model which combine Langmuir and Freundlich models [19, 27]. These models are suitable for predicting adsorption on heterogeneous surfaces (Figure 3).

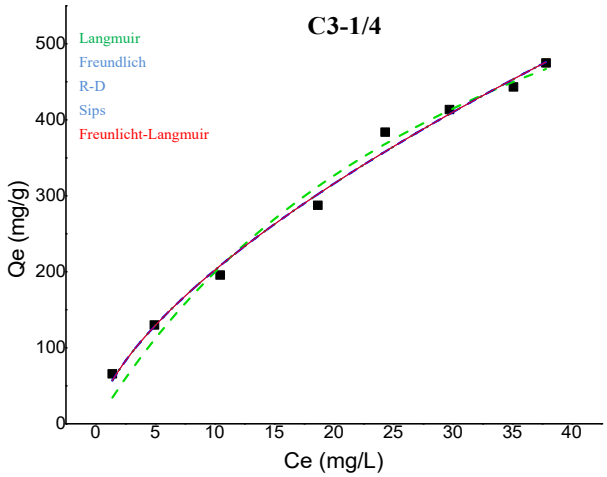

Figure 3. Langmuir, Freunlich, Redlich-Peterson, Sips and Langmuir-Freundlich models applied (nonlinear fit).

Table 4. (a) Isotherm parameters for adsorption of EBT on activated carbon C3-1/4. (b) Non-linear error analysis of isotherm models for the adsorption of EBT onto C3-1/4.

(a)

Models	Constants	Value	R^2
Langmuir	Q_{max} b K_L	902.2 0.02836 0.0555	0.98538
Freundlich	K_F n	45.90 1.5633	0.99252
Redlich-Peterson	a b c	156223 3402 0.3563	0.99252
Sips	Qs Ks β	93549 0.0004895 0.6458	0.99252
Freundlich-Langmuir	Qm K b	124656 4.76×10^{-6} 0.6453	0.99252

(b)

Models	Langmuir	Freundlich	Redlich-Peterson	Sips	Langmuir-Freundlich
SSE	2423	1240	1240	1250	1240
RMSE	20.10	14.37	15.75	15.75	15.75
χ^2	35.19	4.942	4.942	4.990	4.975
HYBRID	355.5	78.80	94.56	95.59	95.12
ARE	10.49	4.594	4.594	4.619	4.617
EABS	116.9	80.57	80.57	80.97	80.64
MPSD	18.85	8.877	9.724	9.777	9.752
SNE	0.9991	0.5234	0.9944	0.9999	0.9971

Adsorption kinetics

The correlation coefficient in general is unsatisfactory for an applicability of the pseudo first order model. The highest value was obtained for a concentration of 0.6 g.L^{-1}. The pseudo second order kinetic model was also applied. The values of Q_{max} are in agreement with the experimental Q_{max} values and those of R^2 (the correlation coefficient): $0.99969 \leq R^2 \leq 1$ when $0.3\ g.L^{-1} \leq C_0 \leq 0.6\ g.L^{-1}$. This model in question is well suited to describe the adsorption process related to the present study (Table 5).

Table 5. Parameters of pseudo first, pseudo second order and Elovich models.

Models	Concentrations			
	0.3 g.L^{-1}	0.4 g.L^{-1}	0.5 g.L^{-1}	0.6 g.L^{-1}
Pseudo-first order				
Qe(mg. g^{-1})	1.683	2.022	13.72	133.28
k1(min^{-1})	0.00179	0.01237	0.06786	0.16603
R^2	0.49892	0.41171	0.48414	0.97521
Pseudo-second order				
Q_{max}(mg. g^{-1})	200	265.96	324.68	401.61
k_2(g.mg^{-1}.min^{-1})	0.04725	0.1043	0.00730	0.0040
h (mg.g^{-1}.min^{-1})	1 890	7 377.63	769.54	645.16
R^2	1	0.99999	0.99969	0.99996
Elovich				
a (mg.g^{-1}.min^{-1})	$0.581*10^{+209}$	$0.1564*10^{+4840}$	$27.36*10^{+35}$	$5.63*10^{9}$
b (g.mg^{-1})	2.434	41.95	0.265	0.06742
Q_e	197.86	265.73	311.3	332.95
R^2	0.6894	0.19911	0.21459	0.67776
$Q_{e,exp}$	198.45	265.45	328.8	399.3

On the other hand, according to the value of the initial adsorption rate h, the mass transfer at the start of the process is maximum for the initial concentration $C_0 = 0.4$ g.L^{-1} in comparison with those of 0.3, 0.5 and 0.6 g.L^{-1}. It is equal to 1890 for 0.3 g.L^{-1}, and then to 7378 for 0.4 g.L^{-1}. Then it decreases for the concentration 0.5 g.L^{-1} and finally reached the minimum value which is equal to 645.2 for the concentration 0.6 g.L^{-1}. First, high values of h indicate that the adsorption process can occur via surface exchange reactions until the functional sites on the surface are fully occupied. Then if it decreases, it will be because of the availability of functional sites at the surface level and/or because of the external resistance to mass transfer and/or because of the diffusion in the pores and/or because of the three phenomenon. The kinetic constants obtained follow the same pattern. Then to check if an activated chemisorption exists or not [19], we also applied the Elovich model. According to the values obtained, chemisorption only appears for the initial concentrations 0.5 g.L^{-1} for $t \leq 10$ min and 0.6 g.L^{-1} for $t \leq 15$ min (the curve Q_t as a function of Log t is a line of the form y = a*x + b with b $\neq$ 0). On the other hand, the correlation coefficient R^2 for the concentrations 0.3, 0.4, 0.5, and 0.6 g.L^{-1} are respectively 0.62728, 0.19911, 0.21459 and 0.67776. So this model is not appropriate to represent the experimental results obtained.

Adsorption mechanism

Not all of the graphs obtained go through the origin so diffusion into the pores is not the kinetically determining step. The plot of Q_t as a function of $t^{0.5}$ (Figure 4) gives two types of graph: a double linearity for the concentrations 0.5 g.L^{-1} and 0.6 g.L^{-1} and one straight line for the concentrations 0.3 g.L^{-1} and 0.4 g.L^{-1}. According to Hammed *et al.* [19, 28, 29], the step representing intraparticle diffusion is only observed for the concentrations 0.5 g. L^{-1} and 0.6 g. L^{-1}. It lasts longer for the 0.6

g.L^{-1}. The transition to the third step corresponding to the adsorption equilibrium is direct for the two remaining concentrations 0.3 g.L^{-1} and 0.4 g.L^{-1} [19]. The results also indicate according to Hameed *et al.* [19] that the first step [19, 27, 28] representing the instantaneous adsorption on the external surface of the adsorbate is the same for the different concentrations. The second step is represented by line which does not pass through the origin so the boundary layer control may be involved in the process [30]. The intercept of the line give C_i: it equal to 258.9 mg/g for 0.5 g/L and 289.9 mg/g for 0.6 g/L. The larger the intercept (value of C_i), the greater the boundary layer effect [29-31].

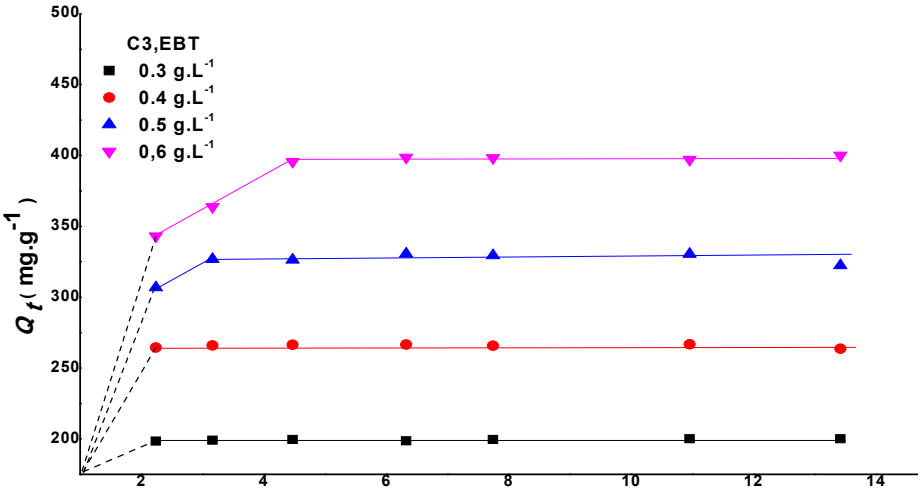

Figure 4. Weber and Morris model.

Thermodynamic studies

Table 6. Thermodynamic adsorption parameters at different temperatures.

Concentration mg.L^{-1}	ΔG				ΔH	ΔS	E_a
	290.7 K	301 K	310 K	323 K			
600	-12.15	-12.2	-11.07	-9.23	-39.92	-0.0938	23.68

ΔG, ΔH and E_a: kJ.mol^{-1}; ΔS: kJ.mol^{-1}.K^{-1}.

From the results obtained (Table 6), free energy is negative at any temperature. So the process is spontaneous. On the other hand, the values of $\Delta H < 0$: it is an exothermic reaction and that of $\Delta S < 0$: the adsorbate-adsorbent system is more ordered than that the initial state. The activation energy E_a was obtained by applying the Arrhenius relation to the results given by the pseudo second order model. After representing $Log\ k_2$ as a function of $1/T$, we have calculated E_a = 23.68 kJ.mol^{-1}: therefore it is a physisorption (< 40 kJ.mol^{-1} [32].

CONCLUSION

The activated carbon was prepared in two stages, in the absence of nitrogen from new lignocellulosic precursor *Asphodelus microcarpus*, under the optimum conditions mentioned above. The yield obtained was 17.5%. The adsorption-desorption of N_2 revealed a mixed porosity, mainly mesoporous, a specific surface area of 1025.8 m^2. g^{-1} and a pore volume of 0.7702 cc.

g^{-1} (C3-1/4). These results make it an ideal adsorbent for the adsorption of a molecule of a dye. Characterization by XRD revealed the presence of only amorphous structure. The SEM showed a heterogenic surface with the presence of pores confirming the results of the adsorption-desorption of N_2. The presence of functional groups on the surface has been identified by the FTIR-ATR technique and the Boehm method. The adsorption of EBT an azo dye which serves as a model follows the pseudo-second order kinetic model and the adsorption isotherm obtained is in agreement with that of Freundlich and also with that of Redlich-Peterson models. Consequently, it can be concluded that this precursor may serve as low-cost potential biomass precursor for the synthesis of activated carbon which could be used as adsorbent for removing anionic and cationic dyes. For a perspective for future work, we will try to develop a micro-meso activated carbon with optimal microporosity.

REFERENCES

1. Buczek, B. Preparation of active carbon additional activation with potassium hydroxide and characterization of their properties. *Adv. Mater. Sci. Eng*. **2016**, 2016, 5819208.
2. Derbyshire, F.J.; Jagtoyen, M. Activated carbon and process for making same. *US Patent* 6,057,262 May 2, **2000**.
3. Marsh, H.; Crawford, D.; O'Grady, T.M.; Wennerberg, A. Carbon of high surface area. Study by adsorption and resolution electron microscopy. *Carbon* **1982**, 20, 419-426.
4. Hui, T.S.; Zaini, M.A.A. Potassium hydroxide activation of activated carbon. *Carbon Lett*. **2015**, 16, 275-280.
5. Oginni, O.; Singh, K.; Oporto, G.; Dawson-Andoh, B.; McDonald, L.; Sabolsky, E. Influence of one-step and two-step KOH activation on activated carbon characteristics. *Bioresour. Technol. Rep.* **2019**, 7, 1-9.
6. Jahan, K.; Singh, V.; Mehrotra, N.; Rathore, K., Verma, V. Development of activated carbon from KOH activation of pre-carbonized *chickpea peel* residue and its performance for removal of synthetic dye from drinking water. *Biomass Convers. Biorefin*. **2023**, 13, 6913-6923.
7. Yahia, E.; Cherif, E.; Ouzzine, M.; Touijer, A.; Coren, F.; Saidi, M. Promising porous carbon material derived from *Argan Paste Cake* by KOH activation, for paracetamol removal. *Processes* **2023**, 11, 1-19.
8. Qui, Z. ; Wang, Y. ; Bi, X. ; Zhou, T. ; Zhou, J.; Zhao, J.; Miao, Z. ; Yi, W.; Fu, P.; Zhuo, S. Biochar based carbons with hierarchical micro-meso-macro porosity for high rate and long cycle life supercapacity. *J. Power Sources* **2018**, 376, 82-90.
9. Evans, M.J.B.; Halliop, E.; MacDonald, J.A.F. The production of chemically activated carbon. *Carbon* **1999***,* 37, 269-274.
10. Benadjemia, M.; Millière, L.; Reinert, L.; Benderdouche, N.; Duclaux, L. Preparation, characterization and methylene blue adsorption of phosphoric acid activated carbon from *globe artichoke* leaves. *Fuel Process. Technol*. **2011**, 92, 1203-1212.
11. Boehm, H.P. Some aspects of the surface chemistry of carbon blacks and other carbons. *Carbon* **1994**, 32, 759-769.
12. Labied, R.; Benturki, O.; Hamitouche, A.; Donnot, A. Adsorption of hexavalent chromium by activated carbon obtained from waste lignocellulosic material (*ziziphus jujube cores*): Kinetic, equilibrium and thermodynamic study. *Adsorpt. Sci. Technol.* **2018**, 36, 1066-1099.
13. Brunauer, S.; Emmet, P.; Teller, E. Adsorption of gases in multimolecular layers. *J. Amer. Chem. Soc.* **1938**, 60, 309-319.
14. De Boer, J.H.; Lippens, B.C.; Linsen, B.G.; Broekhoff, J.C.P.; Van den Heuvel, A.; Osinga, Th.J. The t-curve multimolecular N_2 adsorption. *J. Colloid Interface. Sci*. **1966**, 21, 405-414.
15. Dubinin, M.M.; Stoeckli, H.F. Homogeneous and heterogeneous micropore structures in carbonaceous adsorbents. *J. Colloid Interface Sci*. **1980**, 75, 34-42.

16. Barrett, E.P.; Joyner, L.G.; Halenda, P.P. The determination of pore volume and area distributions in porous substances. I. Computations from nitrogen isotherms. *J. Am. Chem. Soc.* **1951**, 73, 373-380.
17. Foo, K.Y.; Hameed, B.H. Insights into the modeling of adsorption isotherm systems. *Chem. Eng. J*. **2010**, 156, 2-10.
18. Lagergren, S. About the theory of so-called adsorption of soluble substances. *Kungliga Svenska Vetenskapsakademiens Handlingar*. **1898**, 24, 1-39.
19. Hameed, B.H.; Tan, I.A.W.; Ahmad, A.L. Adsorption isotherm, kinetic modeling and mechanism of 2,4,6-trichlorophenol on *coconut husk*-based activated carbon. *Chem. Eng. J.* **2008**, 144, 235-244.
20. Benmessaoud, A.; Nibou, D.; Mekatel, E.; Amokrane, S. A comparative study of the linear and non-linear methods for determination of the optimum equilibrium isotherm for adsorption of Pb^{2+} ions onto Algerian treated clay. *Iran. J. Chem. Chem. Eng.* **2020**, 39, 153-171.
21. Fil, B.A.. Investigation of adsorption of basic orange 2 dye on montmorillonite and error analysis. *Bull. Chem. Soc. Ethiop*. **2023**, 37, 47-58.
22. Dogan, M.; Sabaz, P.; Bicil, Z.; Kizilduman, B.K.; Turhan. Y. Activated carbon synthesis from *tangerine peel* and its use in hydrogen storage. *J. Energy Institute*. **2020**, 93, 2176-2185.
23. Muniandy, L.; Adam, F.; Abdul Rahman, M.; Eng-Poh Ng. The synthesis and characterization of high purity mixed microporous/mesoporous activated carbon from *rice husk* using chemical activation with NaOH and KOH. *Micropor. Mesopor Mater*. **2014**, 197, 316-323.
24. Selvaraju, G.; Abu Bakar, N.K. Production of a new industrially viable green-activated carbon from *Artocarpus integer* fruit processing waste and evaluation of its chemical, morphological and adsorption properties. *J. Cleaner Prod*. **2017**, 141, 989-999.
25. Fu, Y.; Shen, Y.; Zhang, Z.; Ge, X.; Chen, M. Activated bio-chars derived from *rice husk* via one and two-step KOH-catalyzed pyrolysis for phenol adsorption. *Sci. Total Environ.* **2019**, 646, 1567-1577.
26. Ayawei, N.; Ebelegi, A.N.; Wankasi, D. Modelling and interpretation of adsorption isotherms. *J. Chem*. **2017**, 2017, 3039817.
27. Norouzi, S.; Heidari, M.; Alipour, V.; Rahmanian, O.; Fazlzadeh, M.; Mohammadi-moghadam, F.; Nourmoradi, H.; Goudarzi, B. and Dindarloo, K. Preparation, characterization and Cr(VI) adsorption evaluation of NaOH-activated carbon produced from *Date Press Cake*; an agro-industrial waste. *Bioresour. Technol*. **2018**, 258, 48-56.
28. Wu, F.C; Tseng, R.L.; Juang, R.S. Comparisons of porous and adsorption properties of carbons activated by steam and KOH. *J. Colloid Interface Sci.* **2005**, 283, 49-56.
29. Kavitha, D.; Namasivayam, C. Experimental and kinetic studies on methylene blue adsorption by *coir pith* carbon. *Bioresour. Technol.* **2007**, 98, 14-21.
30. Wang, L.; Zhang, J.; Zhao, R. ; Li, C.; Li, Y.; Zhang, C. Adsorption of basic dyes on activated carbon prepared from *Polygonum orientale* Linn: Equilibrium, kinetic and thermodynamic studies. *Desalination* **2010**, 254, 68-74.
31. Muhammad, B.; Javed, A.; Nousahd, H.; Muhammad, U.; Shaukat, S.; Daud, A. Removal of Pb(II) from wastewater using activated carbon prepared from the seeds of *Reptonia buxifolia*. *J. Serb. Chem. Soc.* **2020**, 85, 265-277.
32. Ahmad, M.A.; Herawan, S.G.; Yusof, A.A. Equilibrium, kinetics, and thermodynamics of remazol brilliant blue R dye adsorption onto activated carbon prepared from *Pinang Frond*. *ISRN Mechanical Eng.* **2014**, 3, 1-7.